Generation and propagation of an anomalous vortex beam

Yuanjie Yang,[1] Yuan Dong,[2] Chengliang Zhao,[2,3] and Yangjian Cai[2,4]

[1]*School of Astronautics & Aeronautics, University of Electronic Science and Technology of China, Chengdu 611731, China*

[2]*School of Physical Science and Technology, Soochow University, Suzhou 215006, China*

[3]*e-mail: zhaochengliang@suda.edu.cn*

[4]*e-mail: yangjiancai@suda.edu.cn*

Received September 16, 2013; revised November 6, 2013; accepted November 14, 2013;
posted November 15, 2013 (Doc. ID 197798); published December 11, 2013

A theoretical model is proposed to describe a novel vortex beam named anomalous vortex (AV) beam. Analytical propagation formula for the proposed beam passing through a paraxial ABCD optical system is derived, and the propagation properties of such beam in free space are studied numerically. It is interesting to find that an AV beam will eventually become an elegant Laguerre–Gaussian beam in the far field (or in the focal plane) in free space. Furthermore, we report experimental generation of an AV beam and measure its propagation properties. Our experimental results are consistent with the theoretical predictions. © 2013 Optical Society of America

OCIS codes: (050.4865) Optical vortices; (350.5500) Propagation; (070.2590) ABCD transforms.
http://dx.doi.org/10.1364/OL.38.005418

All forms of waves can contain phase singularities, and the rotational flows around the singular points are called vortices [1]. In a light wave, the phase singularity is known to form an optical vortex. At the center of the optical vortex, the intensity is zero and the phase is undetermined. An optical vortex with an azimuthal phase $\exp(im\varphi)$ may carry an orbital angular momentum of $m\hbar$ per photon, where m denotes the topological charge (azimuthal mode) of the field and also denotes the number of 2π phase cycles around the optical vortex centered on the optical axis, φ is the azimuthal angle about the optical axis z, and $\hbar$ is Planck's constant h divided by 2π [2]. Due to the unique natures of vortex fields, such as a helical wavefront and spatial propagation invariance, optical vortex beams have been used in free-space information transfer and communications [3], quantum information processing and quantum cryptography [4], and optical manipulation [5]. Therefore, the study of optical vortices is important from the viewpoint of not only fundamental but applied physics [4,6].

On the other hand, the elegant Laguerre–Gaussian (ELG) beam is of great importance and has attracted considerable attention since it was introduced in optics [7–13]. However, it is noted that the ELG beams do not represent the modes of a stable spherical-mirror optical resonator, and all the aforementioned studies were carried out theoretically. To our knowledge, the experimental generation of the ELG beam has not been reported yet.

In this Letter, we introduce a novel vortex beam named anomalous vortex (AV) beam, which exhibits unique propagation properties, i.e., the AV beam becomes an ELG beam in the far field (or in the focal plane) in free space. We also carry out experimental generation of an AV beam, and demonstrate experimentally that the generated AV beam indeed becomes an ELG beam in the focal plane. Thus, generation of an AV beam provides one way for generating an ELG beam.

The electric field of the proposed AV beam at $z = 0$ is defined as follows:

$$E_{n,m}(\rho_0, \theta_0, 0) = E_0 \left(\frac{\rho_0}{w_0}\right)^{2n+|m|} \exp\left(-\frac{\rho_0^2}{w_0^2}\right) \exp(-im\theta_0), \tag{1}$$

where E_0 is a constant, n is the beam order of the AVB, m is the topological charge, and w_0 is beam waist size of the fundamental Gaussian beam ($m = n = 0$), ρ_0 and θ_0 are radial and azimuthal coordinates, respectively. When $m = 0$ and $n \neq 0$, Eq. (1) reduces to the electric field for a hollow Gaussian beams [14]. When $n = 0$ and $m \neq 0$, Eq. (1) reduces to the electric field for an ordinary Gaussian vortex beam.

The electric field of the AV beam at $z = 0$ can be expanded as a superposition of a series of Laguerre–Gaussian modes, i.e.,

$$E_{n,m}(\rho_0, \theta_0, 0) = E_0 \frac{n!}{2^n} \sum_{s=0}^{n} (-1)^s \binom{n}{s} L_s\left(\frac{2\rho_0^2}{w_0^2}\right) \times \exp\left(-\frac{\rho_0^2}{w_0^2}\right) \left(\frac{\rho_0}{w_0}\right)^{|m|} \exp(-im\theta_0). \tag{2}$$

Figure 1 shows the intensity distribution (contour graph) of an AV beam for different values of m and n with $w_0 = 1$ mm. From Fig. 1, one finds that the area of the dark region across the AV beam increases as the parameter m or n increases.

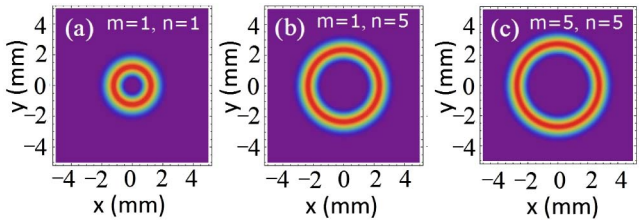

Fig. 1. Intensity distribution (contour graph) of an AV beam for different values of m and n with $w_0 = 1$ mm.

Within the framework of paraxial approximation, the propagation of an AV beam through a stigmatic ABCD optical system can be studied with the help of the following Collins integral [15]:

$$E_{n,m}(\rho,\theta,z) = \frac{i}{\lambda B}\exp(-ikz)\int_0^{2\pi}\int_0^{\infty} E_{n,m}(\rho_0,\theta_0,0) \exp\left\{-\frac{ik}{2B}\times[A\rho_0^2 - 2\rho\rho_0\cos(\theta-\theta_0) + D\rho^2]\right\}\rho_0 \mathrm{d}\rho_0 \mathrm{d}\theta_0, \tag{3}$$

where ρ and θ are radial and azimuthal coordinates in the output plane, A, B, C, and D are the transfer matrices of the paraxial optical system, $k = 2\pi/\lambda$ is the wave number with λ being the wavelength.

Substituting Eq. (1) into Eq. (3), we obtain the following expression for the electric field of the AV beam in the output plane:

$$E_{n,m}(\rho,\theta,z) = \frac{i^{m+1}\pi n!}{\lambda B}\exp\left(-\frac{ik}{2B}D\rho^2 - ikz\right)g^{-(n+|m|+1)}\left(\frac{k\rho}{2B}\right)^{|m|} \times \exp\left(-\frac{k^2\rho^2}{4gB^2}\right)L_n^{|m|}\left(\frac{k^2\rho^2}{4gB^2}\right)\exp(-im\theta), \tag{4}$$

where $L_n^{|m|}(\cdot)$ denotes the Laguerre polynomial of order $|m|$ and n, and

$$g = \frac{1}{w_0^2} + \frac{ikA}{2B}. \tag{5}$$

In the above derivations, we have used the following integral formulas [16]:

$$\int_0^{2\pi}\exp[-in\theta_1 + ikbr\cos(\theta_1-\theta_2)]\mathrm{d}\theta_1 = 2\pi\exp[in(\pi/2-\theta_2)]J_n(kbr), \tag{6}$$

$$\int_0^{\infty}\exp(-ax^2)J_v(2bx)x^{2n+v+1}\mathrm{d}x = \frac{n!}{2}b^v a^{-n-v-1}\exp(-b^2/a)L_n^v(b^2/a). \tag{7}$$

Equation (4) is the main analytical result of this Letter and it provides a convenient tool for studying the propagation and transformation of the AV beam.

The transfer matrix for free space of distance z reads as

$$\begin{pmatrix} A & B \\ C & D \end{pmatrix} = \begin{pmatrix} 1 & z \\ 0 & 1 \end{pmatrix}. \tag{8}$$

Substituting Eq. (8) into Eq. (4) and using the far-field approximation ($z \gg kw_0^2/2$), Eq. (4) reduces to

$$E_{n,m}(\rho,\theta,z) = \frac{i^{m+1}\pi n!}{\lambda z}\exp(-ikz)w_0^{2(n+|m|+1)}\left(\frac{k\rho}{2z}\right)^{|m|} \times \exp\left(-\frac{w_0^2k^2\rho^2}{4z^2}\right)L_n^{|m|}\left(\frac{w_0^2k^2\rho^2}{4z^2}\right)\exp(-im\theta) = \frac{i^{m+1}\pi n!}{\lambda z}\exp(-ikz)w_0^{2n+|m|+2}\exp(-im\theta) \times \left(\frac{\rho}{w}\right)^{|m|}\exp\left(-\frac{\rho^2}{w^2}\right)L_n^{|m|}\left(\frac{\rho^2}{w^2}\right), \tag{9}$$

where $w = zw_0/z_R$ and $z_R = kw_0^2/2$ with w and z_R being the spot radius of the beam at z and the Rayleigh range, respectively.

One finds from Eq. (9) that the electric field of an AV beam in the far field in free space evolves into the electric field of an ELG beam, which means we can use an AV beam as a virtual source to generate an ELG beam. We calculate in Fig. 2 the normalized 3D intensity distribution, the corresponding contour graph and the phase distribution (bottom) of an AV beam at different propagation distances in free space with $w_0 = 1$ mm, $\lambda = 632.8$ nm, and $m = n = 3$. One finds from Fig. 2 that the AV beam has a doughnut profile and a helical phase in the source plane ($z = 0$). Although the dark region decreases with the increase of the propagation distance, the AV beam maintains the profile of a single ring in the near field [Fig. 2(b)]. However, in the far field, the beam profile and the phase structure of the AV beam are much different from those in the near field [see Figs. 2(c), 2(f), and 2(i)]. From Figs. 2(c) and 2(f), we can see that dark rings appear in the intensity distribution. Accordingly, ring dislocations appear in the phase distribution as well [Fig. 2(i)]. Furthermore, Fig. 2(i) shows there are three ring dislocations in the phase plot,

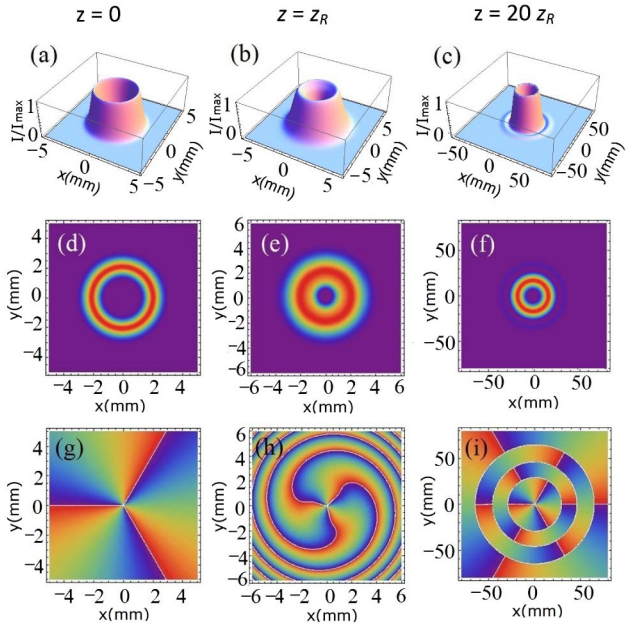

Fig. 2. Normalized 3D intensity distribution (top), the corresponding contour graph (middle), and the phase distribution (bottom) of an AV beam at different propagation distances in free space (a), (d), (g) $z = 0$; (b), (e), (h) $z = z_R$; and (c), (f), (i) $z = 20z_R$.

which indicates that Fig. 2(f) has three dark rings and four bright rings though it is hard to recognize the outer rings.

Now we carry out experimental generation of an AV beam and measure its focused intensity, due to the fact that the beam profile of the far-field intensity is equivalent to that in the focal plane [17]. Figure 3 shows our experimental setup for generating the AV beam and measuring its focused intensity. The laser beam generated by a diode-pumped solid-state laser ($\lambda = 532$ nm) first passes through a neutral density filter, which is used to adjust the power of the beam in order to avoid saturation of the beam profile analyzer (BPA), then it is expanded and collimated by a pair of thin lenses (L_1, L_2). The transmitted beam goes toward a spatial light modulator (SLM) (Holoeye, LC2002), which acts as a grating pattern designed by the method of computer-generated holograms controlled by the PC_1. The grating pattern of holograms was obtained by the interference of a plane wave and an anomalous hollow beam whose electric field is expressed as

$$E_{n,m}^{(0)}(\rho_0, \theta_0, 0) = E_0 \left(\frac{\rho_0}{w_0}\right)^{2n+|m|} \exp\left(-\frac{\rho_0^2}{w_0^2}\right). \qquad (10)$$

Therefore, the first-order diffraction pattern of the beam from the SLM can be regarded as an anomalous hollow beam whose electric field is described by Eq. (10). The anomalous hollow beam, selected by the circular aperture, illuminates a spiral phase plate (SPP) and the transmitted beam can be regarded as the AV beam whose electric field is described by Eq. (1). The transmitted beam just behind the SPP is set as the AV beam source. The generated AV beam just behind the SPP has the same intensity distribution with the generated anomalous hollow beam just before the SPP. In order to study the focusing properties of the generated AV beam, a thin lens L_3 with focal length $f = 400$ mm is located behind the SPP (i.e., in the source plane). After passing through the thin lens L_3, the generated AV beam arrives at the BPA, which is located at the focal plane and is used to measure the focused intensity. The intensity of the generated AV beam in the source plane is also measured by the BPA.

Figure 4 shows our experimental results and the corresponding theoretical results of the intensity distribution of the generated AV beam both at the source plane and the focal plane for different values of m and n. From Figs. 4(a-1) to 4(c-1) and Figs. 4(a-2) to 4(c-2) one can see that the dark size of the beam spot increases with the increase of the parameter m or n in the source plane as expected by Fig. 1. From Figs. 4(a-3) to 4(c-3) and Figs. 4(a-4) to 4(c-4), we find that in the focal plane the size of the beam spot increases with the increase of m or the decrease of n. Our experimental results are consistent with the theoretical predictions; in other words, the AV beam in the focal plane (or in the far field) indeed evolves into an ELG beam. Thus, we can use the AV beam as a virtual source to generate an ELG beam.

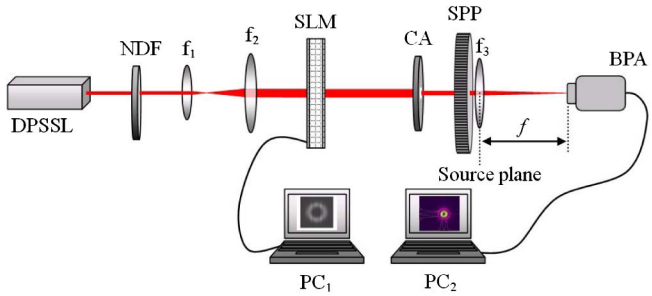

Fig. 3. Experimental setup for generating an AV beam and measuring its focused intensity. DPSSL, diode-pumped solid-state laser; NDF, neutral density filter; L_1,L_2, L_3, thin lenses; SLM, spatial light modulator; CA, circular aperture; SPP, spiral phase plate; BPA, beam profile analyzer; PC_1, PC_2, personal computer.

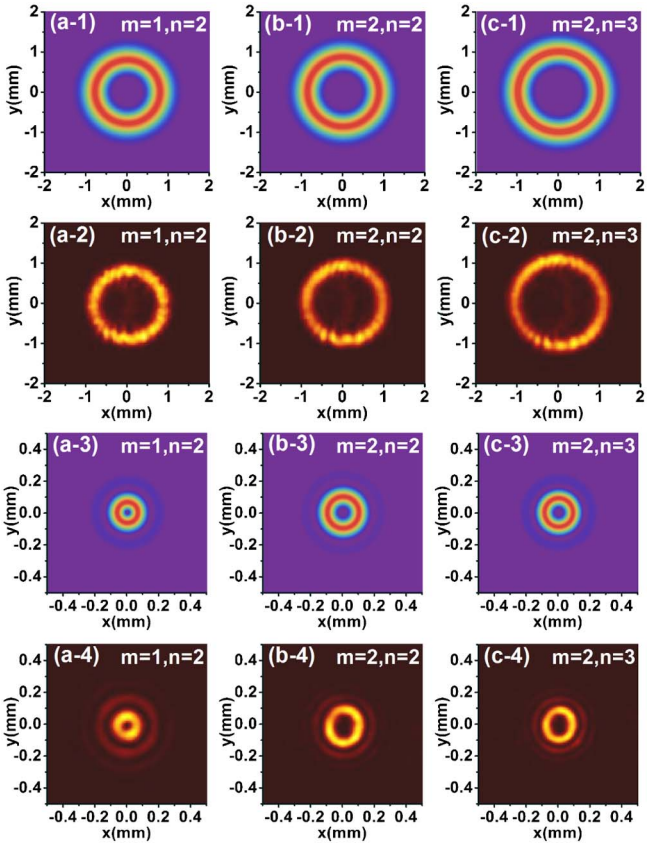

Fig. 4. Theoretical and experimental results of the intensity distribution of the generated AV beam in the source plane [(a-1) to (c-1) and (a-2) to (c-2)] and focal plane [(a-3) to (c-3) and (a-4) to (c-4)] for different values of m and n.

Furthermore, it has been reported that the ELG beams with high radial order n are asymptotically equal to the Bessel–Gauss vortex beams, and even can be identified with Bessel vortex beam in the limit $n \to \infty$ [10]. Therefore, the AV beam can be considered as a virtual source that generates Bessel–Gauss vortex beam and Bessel vortex beam as well.

In conclusion, we have introduced a new kind of vortex beam named AV beam and have derived the analytical propagation formula for such beam passing through a paraxial stigmatic ABCD optical system. Furthermore, we have carried out experimental generation of an AV beam and measured its focusing properties. Both theoretical and experimental results have shown that an AV beam will evolve into an ELG beam in the far field (or in the focal plane) in free space. Thus, the AV beam can be considered as a virtual source for generating an

ELG beam. Due to its unique propagation properties, the AV beam may find applications in optical manipulation and atom guiding.

This work is supported by the National Natural Science Foundation of China under grants 61008009, 11274005, 61205122, and 11374222, the Fundamental Research Funds for the Central Universities under grant ZYGX2010J112, the Huo Ying Dong Education Foundation of China under grant 121009, the Key Project of Chinese Ministry of Education under grant 210081, and the Scientific Research Foundation for the Returned Overseas Chinese Scholars, State Education Ministry.

References

1. M. Uchida and A. Tonomura, Nature **464**, 737 (2010).
2. L. Allen, M. W. Beijersbergen, R. J. C. Spreeuw, and J. P. Woerdman, Phys. Rev. A **45**, 8185 (1992).
3. J. Wang, J. Yang, I. Fazal, N. Ahmed, Y. Yan, H. Huang, Y. Ren, Y. Yue, S. Dolinar, M. Tur, and A. Willner, Nat. Photonics **6**, 488 (2012).
4. G. Molina-Terriza, J. P. Torres, and L. Torner, Nat. Phys. **3**, 305 (2007).
5. K. Dholakia and T. Cizmar, Nat. Photonics **5**, 335 (2011).
6. Y. Yang, M. Mazilu, and K. Dholakia, Opt. Lett. **37**, 4949 (2012).
7. A. E. Siegman, J. Opt. Soc. Am. **63**, 1093 (1973).
8. S. Saghafi and C. J. R. Sheppard, J. Mod. Opt. **45**, 1999 (1998).
9. W. Nasalski, Opt. Lett. **38**, 809 (2013).
10. M. A. Porras, R. Borghi, and M. Santarsiero, J. Opt. Soc. Am. A **18**, 177 (2001).
11. A. April, Opt. Lett. **33**, 1392 (2008).
12. M. A. Bandres and J. C. Gutiérrez-Vega, Opt. Lett. **29**, 2213 (2004).
13. C. Zhao and Y. Cai, Opt. Lett. **36**, 2251 (2011).
14. Y. Cai, X. Lu, and Q. Lin, Opt. Lett. **28**, 1084 (2003).
15. S. A. Collins, J. Opt. Soc. Am. **60**, 1168 (1970).
16. A. Erdelyi, W. Magnus, and F. Oberhettinger, *Tables of Integral Transforms* (McGraw-Hill, 1954).
17. E. Hecht, *Optics*, 4th ed. (Addison-Wesley, 2002).